Microscopic analysis of spin-momentum locking on a geometric phase metasurface

Fernando Lorén [●],[1,2] Gian L. Paravicini-Bagliani,[3] Sudipta Saha,[3] Jérôme Gautier [●],[3] Minghao Li [●],[3]
Cyriaque Genet [●],[3,*] and Luis Martín-Moreno [●][1,2,†]

[1]*Instituto de Nanociencia y Materiales de Aragón (INMA), CSIC-Universidad de Zaragoza, 50009 Zaragoza, Spain*
[2]*Departamento de Física de la Materia Condensada, Universidad de Zaragoza, 50009 Zaragoza, Spain*
[3]*University of Strasbourg and CNRS, CESQ & ISIS (UMR 7006), 8, allée G. Monge, 67000 Strasbourg, France*

We revisit spin-orbit coupling in a plasmonic Berry metasurface composed of rotated nanoapertures, which is known to imprint a robust far-field polarization response. We present a scattering formalism that shows how that spin-momentum locking emerges from the geometry of the unit cell without requiring global rotation symmetries. We find and confirm with Mueller polarimetry measurements that spin-momentum locking is an approximate symmetry. The symmetry breakdown is ascribed to the elliptical projection of circularly polarized light into the planar surface. This breakdown is maximal when surface waves are excited, and a new set of spin-momentum locking rules is presented for this case.

I. INTRODUCTION

Chiral light-matter interactions [1,2] form the core of recent discussions in quantum optics and material science. Recently, such interactions have been investigated in nano-optics, with the appropriate designs of two-dimensional nanoantennas or plasmonic arrays [3–5]. Chiral metasurfaces, sometimes known as "Berry" or "geometric phase metasurfaces" (GPM) [6], have found many applications for the selective manipulation of quantum emitters, in particular in the field of valleytronics [7–9]. There valley excitons can be selectively excited and detected by the spin angular momentum of the emitted light due to the metasurface's spin-momentum locking (SML) mechanism. This allows routing valley degrees of freedom into optical cavity modes, opening ways for new valley-photon interfaces [10–12].

Despite their applicative potential and the fascinating connections they draw with many fundamental issues in optics, plasmonic GPMs have been elusive to a rigorous and exhaustive theoretical description. Previous theoretical works have either considered (i) Berry-phase arguments in systems with optical elements presenting a *continuous* spatial modulation [6] or (ii) a group theory analysis in the Kagome lattice, restricted to waves with an electric field perpendicular to the surface, that ascribed SML to the simultaneous presence of translation and rotation symmetries of the *whole* lattice [3]. None of these approaches cover the typical case of GPMs, which are composed of discrete elements that present chirality within the unit cell but without global rotation symmetries [4,11,13].

Another issue that has not yet been addressed is how SML, which distinguishes between two circular polarization states, can be reconciled with the surface plasmon polariton (SPP),

which only exists for TM polarization. In other words, a strict SML rule implies that all Bragg modes, including surface waves, must have a well-defined circular polarization, which is not possible when the Bragg mode is an SPP.

In this article, we propose a scattering formulation that clarifies how SML appears in a plasmonic holey GPM. Our formulation has three strong assets with respect to previous theoretical works. First, it shows that the SML appears from the geometry of the unit cell. Second, it demonstrates that the SML rules are only approximate when predicting polarization, due to the elliptical projection onto the GPM of the circularly polarized diffraction orders. Third, it enables a direct comparison with experimental data. The validity of our findings is confirmed by the excellent agreement between theory and new experimental data of the polarization states associated with each of the diffracted Bragg modes, determined via Mueller polarimetry performed in the optical Fourier space.

II. THEORETICAL FORMALISM

We consider the simplest GPM, characterized by a periodic array of rectangular grooves in a metal slab. Figure 1(a) presents an SEM image of the periodic gold metasurface that we will experimentally study later, and Fig. 1(b) is a schematic representation of the unit cell, which comprises N grooves, and is periodically repeated in both $\vec{u}_x$ and $\vec{u}_y$ directions. Each groove has a short side a, a long side b, and depth d. The αth groove is rotated at an angle θ_α with respect to the $\vec{u}_x$ axis.

In this paper, we present a general theoretical framework for arbitrary groove positions and θ_α, but we will analyze the case where (i) the groove centers are aligned along the $\vec{u}_x$ axis, (ii) the distance between the centers of nearest grooves is L, in both x and y directions, and (iii) θ_α varies linearly with α, $\theta_\alpha = 2\pi n_w \alpha / N$.

The winding number n_w defines the number of complete 2π rotations along the unit cell (in the particular case $n_w = 0$,

*genet@unistra.fr
†lmm@unizar.es
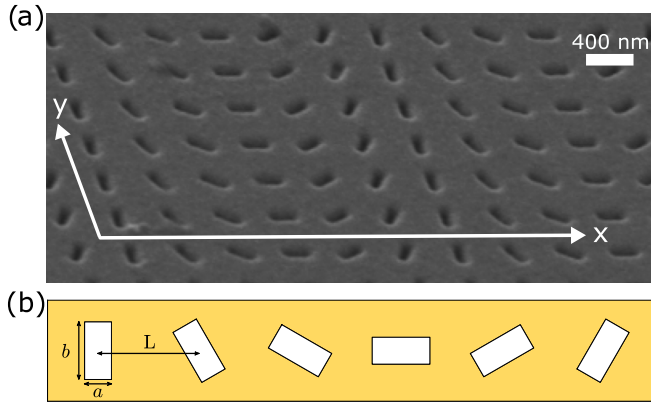
FIG. 1. (a) Scanning electron microscope (SEM) image of the periodic metasurface, composed of rectangular grooves in a gold film. (b) Schematic bird's-eye view of the unit cell. Nominal parameters in panel (a): $a = 80$ nm, $b = 220$ nm, $d = 60$ nm, and $L = 460$ nm.

the array becomes a nonchiral square lattice of rectangular grooves). The system depicted in Fig. 1(b) has $n_w = 1/2$, as each rectangular groove presents a mirror symmetry with respect to the middle of the long axis. Consequently, the rotation along one unit cell is only of π radians because the next unit cell is the same and completes the 2π rotation. Notice that, generally, a surface characterized by a constant increment in angle θ from hole to hole requires an integer n_w. However, a rectangular aperture has reflection symmetry along its long axis, which makes the collection of holes repeat itself already for $n_w = 1/2$, thus halving the unit cell size (if holes depicted in Fig. 1(b) were trapezoidal, the unit cell would comprise 12 holes while the structure repeats itself already after six rectangular holes). Notice also that although the grooves perform a stepwise rotation within the unit cell, the whole lattice does not support a global rotation symmetry.

We consider an electromagnetic plane wave impinging onto the structure with an in-plane wave vector along the x direction, $\vec{k}^{in} = k_x^{in}\vec{u}_x$, and compute the reflection coefficients into the different Bragg modes that can be diffracted off the periodic metasurface. For that, we use the coupled-mode method (CMM), which has been widely used in the study of electromagnetic (EM) properties in holey metallic films [14]. The CMM expands the EM fields in plane waves in the free space regions and waveguide modes inside the grooves and finds the field amplitudes by adequately matching the fields at the interfaces.

The equations derived from the CMM are usually written in terms of the amplitudes of the waveguide modes [15–17]. However, when studying the SML mechanism, we find it more convenient to derive the equations directly for the reflection coefficients. Although computationally less efficient, this provides a more transparent description as it now involves far-field amplitudes, thus avoiding the near-field to far-field decoding needed to extract scattering coefficients from waveguide mode amplitudes.

Bragg modes are characterized by an in-plane momentum $\vec{k} = \vec{k}^{in} + \vec{G}$, where $\vec{G}$ is a reciprocal lattice vector, in this case $\vec{G} = 2\pi m/(NL)\vec{u}_x + 2\pi n_y/L\vec{u}_y$, where m and n_y are

integers. To develop a minimal model for studying the SML and simplify the presentation, in the main text, we consider only Bragg modes with $n_y = 0$. As shown in Sec. 2 in the Supplemental Material [18], this does not change the main results because along the y axis there is no breaking of inversion symmetry. We collect the two circular polarizations for the reflected mth Bragg mode in the spinor $\mathbf{r}_m \equiv (r_m^+, r_m^-)^T$, where $\pm$ denote the right- and left-handed polarizations, each of them defined within the plane perpendicular to the wave vector of the corresponding Bragg mode, $\vec{k}_m$. We choose the spin representation because the spin of a plane wave is conserved on reflection by a mirror [19–22] (while the helicity changes sign).

The CMM can take into account the dielectric constant in the metal via the implementation of the surface impedance boundary conditions (SIBC). The general expressions can be found in Sec. 1 in Supplemental Material [18] and are the ones used below when comparing to the experimental data. Here we present the expressions for the simpler case in which the metal is treated as a perfect electric conductor (PEC), as this is sufficient to discuss the physics and the structure of the equations:

$$\mathbf{r}_m = -\delta_{m0}\,\mathbf{i}_0 + C_{m0}\,Y_0\,\mathbf{i}_0 - \sum_{m'} C_{mm'}\,Y_{m'}\,\mathbf{r}_{m'}. \tag{1}$$

The first term takes into account the specular reflection ($\mathbf{i}_0$ is the amplitude of the incident wave). The coefficients $C_{mm'}$, which we call "geometric couplings," are 2×2 matrices operating in polarization space. They couple different Bragg modes via scattering with the GPM and encode the geometry of the unit cell through the overlaps between Bragg and waveguide modes (see Sec. 1 in Supplemental Material [18]). That is, they contain the information on the geometric distribution of the holes in the unit cell and thus on whether they are rotated or not. Y_m are the modal admittance matrices of the Bragg modes in the circular polarization basis (which relate the in-plane magnetic field to the electric one). They can be written as $Y_m = \bar{Y}_m \mathbb{1} + \Delta_m \sigma_x$, where $\mathbb{1}$ and σ_x are the 2×2 unit matrix and the Pauli matrix that swaps spin states, respectively. In terms of the linear p (transverse magnetic) $- s$ (transverse electric) polarized basis, $\bar{Y}_m \equiv (Y_{mp} + Y_{ms})/2$ and $\Delta_m \equiv (Y_{mp} - Y_{ms})/2$. For a plane wave with frequency ω and in-plane wave vector k_m propagating in a uniform medium with dielectric constant ϵ, $Y_{mp} = \epsilon/q_{mz}$ and $Y_{ms} = q_{mz}$, where $q_{mz} = \sqrt{\epsilon - (ck_m/\omega)^2}$ (c being the speed of light).

Notice that $\Delta_0 = 0$ at normal incidence, while both $\bar{Y}_m$ and Δ_m diverge at the Rayleigh points (i.e., whenever a diffractive order becomes tangent to the metal-dielectric interface, as then $q_{mz} = 0$).

III. SPIN-MOMENTUM LOCKING

The geometric couplings have a simple analytical expression when the polarization is defined on the circular basis with respect to the $\vec{u}_z$ direction ($C_{mm'}^z$). When the groove dimensions are much smaller than the wavelength, we find (see Secs. 1 and 3 in the Supplemental Material [18] for detailed

derivation)

$$C_{mm'}^z = C\left(\delta_{m,m'+n_0 N}\mathbb{1} + \sum_{s=\pm}\delta_{m,m'+n_0 N - 2n_w s}\,\sigma_s\right), \quad (2)$$

where C is a constant that only depends on the properties of a single groove, n_0 is an integer, and $\sigma_\pm$ are Pauli matrices that increase and decrease spin, respectively. The expression of the couplings coefficients in the circular polarization basis of each Bragg mode, $C_{mm'}$, can be obtained from $C_{mm'}^z$ using the 2×2 "rotation" matrices $R^{k(m)\leftarrow z}$ and $R^{z\leftarrow k(m')}$:

$$C_{mm'} = R^{k(m)\leftarrow z}\,C_{mm'}^z\,R^{z\leftarrow k(m')}. \quad (3)$$

The expressions for $R^{k(m)\leftarrow z}$ and $R^{z\leftarrow k(m')}$ are provided in Sec. 1 in the Supplemental Material [18].

If all Δ_m were zero and all change of basis matrices R were the identity, which only occurs at the direction normal to the surface, then the previous expressions would give rise to the following Bragg laws. The term proportional to $\mathbb{1}$ in the Eq. (2) preserves spin, $\sigma_{\text{out}} = \sigma_{\text{in}}$, and the associated Bragg law $k_x^{\text{out}} = k_x^{\text{in}} + n_0 G^0$, with $G^0 = 2\pi/L$, would be the same one that would appear if all grooves were parallel (and so it is denoted as "standard" Bragg law [3]). The terms inside the sum in the Eq. (2) swap spin, $\sigma_{\text{out}} = \sigma_{\text{in}} \pm 1$, and shift the standard Bragg law by a term that depends both on the spin change and the winding number: $k_x^{\text{out}} = k_x^{\text{in}} + n_0 G^0 \mp k_g$, where $k_g \equiv 2\pi\, 2n_w/(NL)$ is the geometric momentum. This condition is denoted as spin-orbit Bragg law [3] and corresponds to the exact SML mechanism.

These two Bragg laws have been amply used to discuss experimental results but, as mentioned, they were derived only for the cases of continuous spatial modulation [6] and in a lattice that presents a combination of translation and rotation symmetry of the *whole* lattice [3]. In our treatment, they appear from the groove-mediated geometric couplings between Bragg modes in a system without a global rotational lattice symmetry. Thus, SML is a feature of the basis of the unit cell and not of the symmetry of the whole lattice.

However, $\Delta_m \neq 0$ and $R \neq \mathbb{1}$ for Bragg modes with wave vectors away from the surface normal, so the terms proportional to σ_x in both Y_m and the modifications when passing from $C_{mm'}^z$ to $C_{mm'}$ must be considered. These terms flip circular polarization before the geometric couplings are applied. Thus the symmetry that leads to Eq. (2) still holds, but the exact link between changes in momentum and spin, found when assuming $\Delta_m = 0$ and $R = \mathbb{1}$, breaks down.

The physical origin of the breakdown terms resides in that the polarization of the transversal EM field is defined on the plane *perpendicular to the wave vector*. However, the in-plane component (i.e., *perpendicular to the surface normal*) of the EM field is the relevant one in the interaction with the holey metasurface. This mismatch results in the EM wave being elliptically polarized and thus described by a combination of the two circular polarizations with respect to the propagation direction.

Mathematically, for a PEC, the breakdown term is maximum for waves with $q_{mz} = 0$, while for a real metal, this occurs when the Bragg mode coincides with the SPP *of the flat surface*. Considering SML breakdown terms is thus essential when surface resonances are excited (spoof SPPs in the case
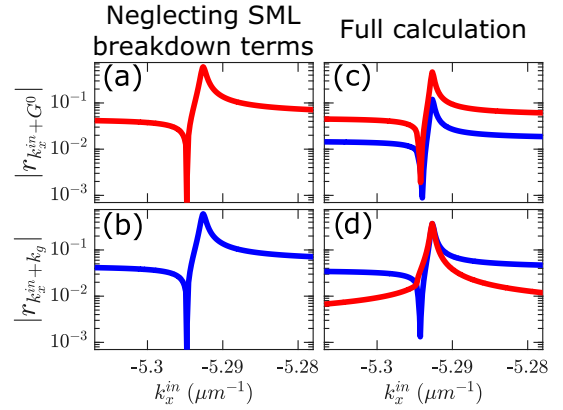
FIG. 2. Reflection coefficients for the two polarizations (spin $+$ in red and spin $-$ in blue) and two different diffraction orders. The incident EM wave has spin $+$ and in-plane momentum k_x^{in}. The chosen resonance is such that $k_x^{\text{SPP}} \approx k_x^{\text{in}} + G^0 + k_g$. [(a) and (b)] Approximate calculation neglecting SML breakdown terms. $r_{k_x^{\text{in}}+G^0} = 0$ for spin $-$ in panel (a) and $r_{k_x^{\text{in}}+k_g} = 0$ for spin $+$ in panel (b). [(c) and (d)] Full calculation, including breakdown terms. Chosen values: $\omega = 2.1$ eV, $a = 80$ nm, $b = 220$ nm, $d = 60$ nm, $L = 460$ nm, $n_w = 1/2$, and $N = 6$, based on the experimental sample shown in Fig. 1. The metal is considered as a PEC.

of a PEC, SPPs of the corrugated surface in the case of a real metal [23]).

To illustrate the relevance of the breakdown terms, we consider an incident left-handed (spin $+$) polarized wave, impinging onto the GPM described in Fig. 1. We compute the reflection coefficients at a fixed frequency as a function of k_x^{in}, near an SPP resonance. Figure 2 renders the results for two different Bragg orders ($r_{k_x^{\text{in}}+G^0}$ and $r_{k_x^{\text{in}}+k_g}$) and the two circular polarizations (spin $+$ in red and spin $-$ in blue). The left panels [Fig. 2(a) and 2(b)] are computed neglecting all breakdown terms by artificially forcing both $\Delta_m = 0$ (taking $Y_{ms} = Y_{mp}$) and $C_{mm'} = C_{mm'}^z$, while the right panels [Figs. 1(c) and 1(d)] are the full calculations including the breakdown terms. As expected, when breakdown terms are neglected, the coefficient $r_{k_x^{\text{in}}+G^0}$ is nonzero only for spin $+$, while the Bragg mode that has gained an extra geometric momentum k_g has an associated spin reduction, and is thus nonzero only for spin $-$. When the breakdown terms are considered, as they should, both polarizations become finite for any Bragg order. Away from the SPP resonance, the effect of the breakdown terms is small and SML selection rules hold to a good approximation. However, the breakdown terms can not be neglected at resonance. So a new set of phenomenological selection rules is needed to understand the SML in plasmonic metasurfaces when SPPs are excited. This will be analyzed in detail in the next section when describing the excitation and deexcitation of SPPs.

Notice that we can apply the geometric couplings sequentially. This is, we can study the couplings between a Bragg mode and a second one, and then the couplings between the latter and another different. This way, the first mode can be coupled to modes with two or more units of added geometric momentum ($\pm 2\,k_g$, $\pm 3\,k_g$, etc.). Of course, this would not be possible if the SML were perfect because spinor algebra

would prevent this process (it is impossible to reduce more than one spin unit to a spin $1/2$). However, as we will show in the next section, breakdown terms enable this remarkable phenomenology.

IV. MUELLER POLARIMETRY

A more detailed analysis of the metasurface's full polarization response can be obtained with Mueller polarimetry that measures, artifact-free, the polarization states of the light beams incident on and scattered off the metasurface. The 4×4 Mueller matrix M is defined by $\mathbf{S}_{\text{out}} = M \, \mathbf{S}_{\text{in}}$, where $\mathbf{S}_{\text{in/out}}$ are the input and output polarization states described by the Stokes vectors [24–26]. Using the experimental scheme presented in Sec. 4 in the Supplemental Material [18], M can be measured as a function of photon energy ω and k_x^{in}. Among the 16 components of the Mueller matrix, we concentrate on the component M_{30}, which provides the difference in reflected intensities between the $+$ and $-$ polarizations when the system is illuminated with unpolarized light.

For a flat interface, in-plane momentum is conserved, and M can be measured for all ω and k_x^{in} at once, using an objective whose back focal plane is fully illuminated with a collimated white light beam. However, the Mueller matrix can be defined and measured for each diffracted order n in a periodically corrugated interface; see Fig. 3(a). Here we will analyze $M_{30}^n(\omega, k_x^{\text{in}})$, obtained from the polarization properties of the reflected light at Bragg orders $k_x^{\text{out}} = k_x^{\text{in}} + n k_g$, and restricting ourselves to $n = 0, 1, 2$, for reasons explained below. The experimental results for the GPM shown in Fig. 1 are presented in Figs. 3(b)–3(d). Panels Figs. 3(e)–3(g) show the numerical simulations performed with the CMM framework within the SIBC approximation. The calculations reproduce the main features found in the experiments. All panels show inverted parabolic features related to the resonant excitation of the SPP of the metasurface.

Let us concentrate on the plasmonic resonances, which are the main reason for analyzing metallic GPMs. We find that *resonant* reflection processes can be understood as two-step scattering processes. First, the incident light scatters with the surface picking up momentum $n_0 G^0 + n_1 k_g$ and adding spin $-n_1$ (where $n_1 = 0, \pm 1$). If this scattered wave is an SPP, then it only has a *p*-polarization component. A subsequent scattering of the SPP with the surface brings it into one of the considered diffraction orders (for that, the picked momentum must be $-n_0 G^0 + n_2 k_g$, which adds spin $-n_2$). Taking into account that the SPP excitation can mathematically be represented as a projector onto the *p*-linear polarization, this two-step resonant scattering process results in the following rules:

$$k_x^{\text{SPP}} = k_x^{\text{in}} + n_0 G^0 + n_1 \, k_g, \tag{4}$$

$$k_x^{\text{out}} = k_x^{\text{in}} + (n_1 + n_2) \, k_g, \tag{5}$$

$$\sigma_{\text{out}} = \sigma_{-n_2} \cdot \mathbf{p} \, (\mathbf{p}^T \cdot \sigma_{-n_1} \cdot \mathbf{i}_0), \tag{6}$$

where $\mathbf{p} = 2^{-1/2} \, (1, 1)^T$ is the linear *p*-polarization and $\mathbf{i}_0$ the incident polarization (in the circular polarization basis), $\sigma_\pm$ are the Pauli matrices that increase and decrease spin,
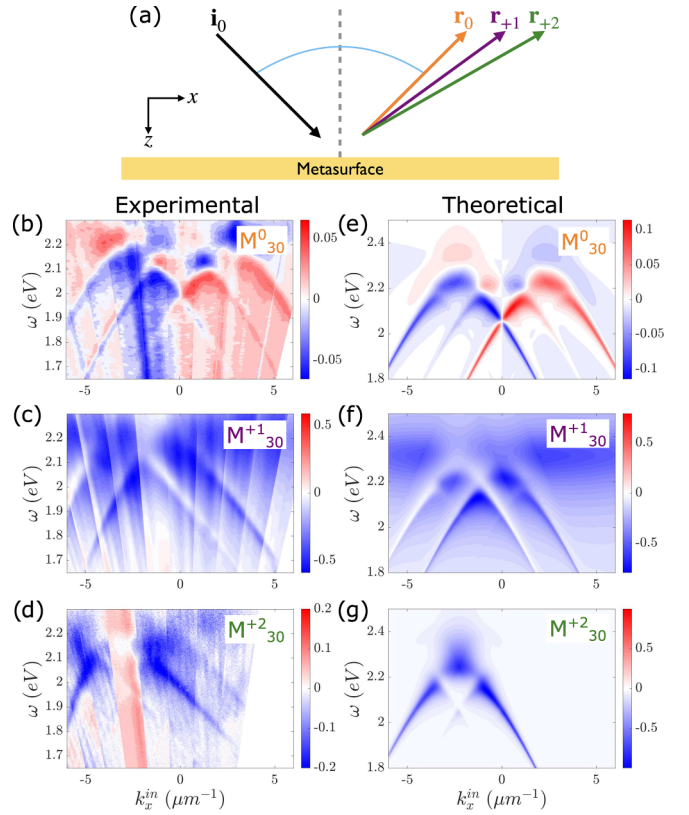
FIG. 3. Mueller polarimetry for the system described in Fig. 1(a). The grooves are filled with SiO$_2$, which also forms a 4-nm layer above the gold metasurface. (a) Scheme of the chosen Bragg modes. [(b)–(d)] Experimental $M_{30}^n(\omega, k_x^{\text{in}})$, for a reflected wave with $k_x^{\text{out}} = k_x^{\text{in}} + n k_g$. [(e)–(g)] Theoretical $M_{30}^n(\omega, k_x^{\text{in}})$. The calculations have been performed within the SIBC approximation, and the groove dimensions have been phenomenologically enlarged by 1.25 times the skin depth to consider the field penetration in the metal [15].

and we have written $\sigma_0 \equiv \mathbb{1}$. These rules substitute the SML rules when SPPs are excited and are the ones to be used to understand and predict the polarization properties of resonant plasmonic structures.

We start by considering how this reasoning applies to the case $k_x^{\text{out}} = k_x^{\text{in}} + k_g$, rendered in Figs. 3(c) and 3(f). The central parabola corresponds to the case $n = 1$, $n_1 = 0$, $n_2 = 1$. As $n_1 = 0$, the unpolarized incident light maintains its spin after interacting with the surface and thus can excite the linearly polarized SPP. The second scattering with the surface removes the $n G^0$ momentum. Still, it adds $+k_g$, thus decreasing the spin of the *p*-polarized wave, ending with spin $-$, which agrees with both experimental and computed results. The parabola that appears displaced to a smaller k_x^{in} arises from the processes $n = 1$, $n_1 = 1$, $n_2 = 0$. Thus the incident photon has spin $-$ after the first scattering, still being able to excite the SPP. As the second scattering with the grating has $n_2 = 0$, it conserves spin, and the reflected photon is linearly polarized (so, it has $M_{30} = 0$, in accordance with the experimental data). Thus, both parabolas involve resonant excitation of an SPP and two interactions with the holey array, described by one standard and one spin-orbit Bragg laws, being the

difference in the order of the "standard" and "geometric" processes.

Figures 3(d) and 3(g) represent the case when the outcoming momentum is $+2k_g$ larger than the incident one. The existence of this diffraction order is a direct confirmation of the presence of the SML breakdown, as an exact SML would imply that the addition of $+2k_g$ momentum must be accompanied by a reduction of spin in -2 units, which is not possible (as $\sigma_-^2 = 0$ for spin 1/2 spinors). In this case, both experiment and calculation show only one plasmonic resonance, resulting in a spin $-$ in the reflected wave. The reason is that the two interactions with the array now involve spin-orbit Bragg laws. The first interaction of the incident wave with the holey surface and the resonant excitation of SPP is like in Figs. 3(c) and 3(f), but the second interaction also adds geometrical momentum and thus decreases spin, producing a reflected wave with spin $-$.

Finally, Figs. 3(b) and 3(e) represent the case of specular reflection: $k_x^{\text{out}} = k_x^{\text{in}}$. In this case, on top of the processes described by Eqs. (4)–(6) the direct reflection [the term $-\delta_{m0}\mathbf{i}_0$ in Eq. (1)] must also be considered, and it dominates the signal. For this reason, spin $-$ is fully reflected in the left parabola while spin $+$, which can couple to an SPP, is only partially reflected. Thus, overall, $M_{30}^0(\omega, k_x^{\text{in}})$ is negative in that spectral region, although much lower in magnitude than for the rest of Bragg orders ($n = 1, 2$) because of the dominance of the specular reflection.

Therefore, we have seen that the SPP acts as a filter to linear p-polarized light and also allows us to reach processes where the photon acquires an extra momentum $2k_g$, which would not be possible without the SML breakdown.

V. CONCLUSION

We have presented a rigorous theoretical analysis, based on a scattering formalism, that shows how spin-momentum locking in geometric phase metasurfaces emerges from the geometry (winding number) of the unit cell. Furthermore, we show that SML is an approximate symmetry with or without global lattice symmetries. SML breakdown terms yield couplings to Bragg orders that would otherwise be uncoupled, such as reflected waves that pick up two units of geometrical momentum. The origin of the SML breakdown is that each circularly polarized wave has an elliptical polarization when projected onto the surface (except for waves with momentum normal to the surface). This breakdown is particularly relevant when linearly polarized surface resonances (as surface plasmon polaritons) are excited. Our analysis shows how SML rules should be modified when surface modes are resonantly excited in the system. This process can be viewed as a two-step interaction with the metasurface, with the plasmon acting as a polarization filter. These modified SML rules perfectly agree with experimental results on the excitation of plasmonic resonances obtained with Mueller polarimetry.

Considering the crucial role played by spin-momentum locking in integrated quantum optical systems [2], our elucidation of the mechanism and its relation to the near-field will help understand and design plasmonic structures for the polarization control of light. This is important in the current applicative perspectives discussed currently in the context of optovalleytronic systems [27], nonlinear hybrid metasurfaces [28], and topology-based high-resolution sensors [29].

[1] K. Y. Bliokh, D. Smirnova, and F. Nori, Science **348**, 1448 (2015).

[2] P. Lodahl, S. Mahmoodian, S. Stobbe, A. Rauschenbeutel, P. Schneeweiss, J. Volz, H. Pichler, and P. Zoller, Nature (Lond.) **541**, 473 (2017).

[3] N. Shitrit, I. Yulevich, E. Maguid, D. Ozeri, D. Veksler, V. Kleiner, and E. Hasman, Science **340**, 724 (2013).

[4] M. Fox and Y. Gorodetski, Appl. Phys. Lett. **120**, 031105 (2022).

[5] K. Bliokh, F. Rodríguez-Fortuño, F. Nori, and A. Zayats, Nat. Photon. **9**, 796 (2015).

[6] Z. Bomzon, G. Biener, V. Kleiner, and E. Hasman, Opt. Lett. **27**, 1141 (2002).

[7] L. Sun, C.-Y. Wang, A. Krasnok, J. Choi, J. Shi, J. S. Gomez-Diaz, A. Zepeda, S. Gwo, C.-K. Shih, A. Alù, and X. Li, Nat. Photon. **13**, 180 (2019).

[8] S. Guddala, R. Bushati, M. Li, A. B. Khanikaev, and V. M. Menon, Opt. Mater. Expr. **9**, 536 (2019).

[9] P. K. Jha, N. Shitrit, X. Ren, Y. Wang, and X. Zhang, Phys. Rev. Lett. **121**, 116102 (2018).

[10] S.-H. Gong, F. Alpeggiani, B. Sciacca, E. C. Garnett, and L. Kuipers, Science **359**, 443 (2018).

[11] T. Chervy, S. Azzini, E. Lorchat, S. Wang, Y. Gorodetski, J. A. Hutchison, S. Berciaud, T. W. Ebbesen, and C. Genet, ACS Photon. **5**, 1281 (2018).

[12] K. Rong, B. Wang, A. Reuven, E. Maguid, B. Cohn, V. Kleiner, S. Katznelson, E. Koren, and E. Hasman, Nat. Nanotechnol. **15**, 927 (2020).

[13] P. Genevet, F. Capasso, F. Aieta, M. Khorasaninejad, and R. Devlin, Optica **4**, 139 (2017).

[14] F. J. Garcia-Vidal, L. Martin-Moreno, T. W. Ebbesen, and L. Kuipers, Rev. Mod. Phys. **82**, 729 (2010).

[15] L. Martín-Moreno, F. J. García-Vidal, H. J. Lezec, K. M. Pellerin, T. Thio, J. B. Pendry, and T. W. Ebbesen, Phys. Rev. Lett. **86**, 1114 (2001).

[16] L. Martín-Moreno and F. J. García-Vidal, J. Phys.: Condens. Matter **20**, 304214 (2008).

[17] F. de León-Pérez, G. Brucoli, F. J. García-Vidal, and L. Martín-Moreno, New J. Phys. **10**, 105017 (2008).

[18] See Supplemental Material at http://link.aps.org/supplemental/10.1103/PhysRevB.107.165128 for (i) the derivations of the CMM equations for a real metal, (ii) the justification for the minimal model used in the text, (iii) the validity of the small-hole approximation, and (iv) theexperimental set-up for Mueller polarimetry, which also includes Refs. [30–32].

[19] K. Y. Bliokh, A. Y. Bekshaev, and F. Nori, New J. Phys. **15**, 033026 (2013).

[20] R. P. Cameron, S. M. Barnett, and A. M. Yao, New J. Phys. **14**, 053050 (2012).

[21] R. P. Cameron, S. M. Barnett, and A. M. Yao, J. Mod. Opt. **61**, 25 (2014).

[22] R. P. Cameron, J. B. Götte, S. M. Barnett, and A. M. Yao, Philos. Trans. R. Soc. Lond. A **375**, 20150433 (2017).

[23] J. B. Pendry, L. Martín-Moreno, and F. J. Garcia-Vidal, Science **305**, 847 (2004).

[24] C. Menzel, C. Rockstuhl, and F. Lederer, Phys. Rev. A **82**, 053811 (2010).

[25] J. J. G. Pérez and R. Ossikovski, *Polarized Light and the Mueller Matrix Approach* (CRC Press, Boca Raton, FL, 2017).

[26] H. Fujiwara, *Spectroscopic Ellipsometry* (John Wiley & Sons, New York, 2007).

[27] M. Li, I. Sinev, F. Benimetskiy, T. Ivanova, E. Khestanova, S. Kiriushechkina, A. Vakulenko, S. Guddala, M. Skolnick, V. M. Menon, D. Krizhanovskii, A. Alù, A. Samusev, and A. B. Khanikaev, Nat. Commun. **12**, 4425 (2021).

[28] G. Hu, X. Hong, K. Wang, J. Wu, H.-X. Xu, W. Zhao, W. Liu, S. Zhang, F. J. García-Vidal, B. Wang, P. Lu, and C.-W. Qiu, Nat. Photon. **13**, 467 (2019).

[29] F. Ding, A. Pors, and S. I. Bozhevolnyi, Rep. Prog. Phys. **81**, 026401 (2018).

[30] A. Thomas, T. Chervy, S. Azzini, M. Li, J. George, C. Genet, and T. W. Ebbesen, J. Phys. Chem. C **122**, 14205 (2018).

[31] E. Lorchat, S. Azzini, T. Chervy, T. Taniguchi, K. Watanabe, T. W. Ebbesen, C. Genet, and S. Berciaud, ACS Photon. **5**, 5047 (2018).

[32] M. Li, Ph.D. thesis, Université de Strasbourg, 2020, https://www.theses.fr/2020STRAF018.